Imaging Myocardial Metabolic Remodeling

Robert J. Gropler[1], Rob S.B. Beanlands[2], Vasken Dilsizian[3], E. Douglas Lewandowski[4], Flordeliza S. Villanueva[5], and Maria Cecilia Ziadi[2]

[1]Division of Radiological Sciences, Edward Mallinckrodt Institute of Radiology, Washington University School of Medicine, St. Louis, Missouri; [2]Molecular Function and Imaging Program and the National Cardiac PET Centre, Division of Cardiology, and the Cardiovascular Research Methods Centre of the University of Ottawa Heart Institute, Ottawa, Ontario, Canada; [3]Division of Nuclear Medicine, Department of Radiology, University of Maryland School of Medicine, Baltimore, Maryland; [4]Program in Integrative Cardiac Metabolism, Center for Cardiovascular Research, University of Illinois at Chicago College of Medicine, Chicago, Illinois; and [5]Cardiovascular Institute and Center for Ultrasound Molecular Imaging and Therapeutics, University of Pittsburgh, Pittsburgh, Pennsylvania

Myocardial metabolic remodeling is the process in which the heart loses its ability to utilize different substrates, becoming dependent primarily on the metabolism of a single substrate such as glucose or fatty acids for energy production. Myocardial metabolic remodeling is central to the pathogenesis of a variety of cardiac disease processes such as left ventricular hypertrophy, myocardial ischemia, and diabetic cardiomyopathy. As a consequence, there is a growing demand for accurate noninvasive imaging approaches of various aspects of myocardial substrate metabolism that can be performed in both humans and small-animal models of disease, facilitating the crosstalk between the bedside and the bench and leading to improved patient management paradigms. SPECT, PET, and MR spectroscopy are the most commonly used imaging techniques. Discussed in this review are the strengths and weaknesses of these various imaging methods and how they are furthering our understanding of the role of myocardial remodeling in cardiovascular disease. In addition, the role of ultrasound to detect the inflammatory response to myocardial ischemia will be discussed.

Key Words: cardiology (basic/technical); molecular imaging; PET; myocardial imaging; myocardial metabolic remodeling; myocardial repair

J Nucl Med 2010; 51:88S–101S
DOI: 10.2967/jnumed.109.068197

As expertly highlighted in the previous review by Taegtmeyer (*1*), flexibility in myocardial substrate metabolism is fundamental to cardiac health. The ability of the heart to modify the type of substrate it metabolizes is critical to maintain a proper balance between myocardial energy production and function in response to various stimuli such as alterations in the plasma substrate or hormonal environment, myocardial blood flow, and cardiac work. The loss in flexibility leads to an overdependence on the metabolism of an individual category of substrates, such as fatty acids or carbohydrates, that can initiate a cascade of events detrimental to myocellular health, including impaired myocardial energetics, stimulation of cellular inflammation and oxidative stress, and enhancement of both cell growth and cell death pathways, resulting in reduced myocardial systolic and diastolic function. Indeed, this metabolic remodeling process is central to the pathogenesis of a variety of cardiac disease processes such as left ventricular hypertrophy, myocardial ischemia, and diabetic cardiomyopathy. However, important unresolved questions remain, including, what are the key determinants of these metabolic perturbations in relation to specific diseases, do they alter prognosis, and do they represent robust targets for novel therapeutics? As a consequence, the demand is growing for accurate noninvasive imaging approaches of various aspects of myocardial substrate metabolism that can be performed in both humans and small-animal models of disease, facilitating the crosstalk between the bedside and the bench and leading to improved patient management paradigms. This article discusses these various imaging methods and how they are furthering our understanding of the role of myocardial remodeling in cardiovascular disease. In addition, the role of ultrasound to detect the inflammatory response to myocardial ischemia is discussed.

Received Feb. 26, 2010; revision accepted Apr. 12, 2010.
For correspondence or reprints contact: Robert J. Gropler, Cardiovascular Imaging Laboratory, Mallinckrodt Institute of Radiology, 510 S. Kingshighway, St. Louis, MO 63110.
E-mail: Groplerr@mir.wustl.edu

METHODS TO IMAGE MYOCARDIAL METABOLISM

Several methods are available to image myocardial metabolism noninvasively; the most common are SPECT, PET, and MR spectroscopy (MRS).

SPECT

An advantage of SPECT is the inherent high sensitivity of the radionuclide method to measure metabolic processes. Moreover, the technology is widely available in both the clinical and research settings. Theoretically, assessing more than one metabolic process simultaneously is possible if the heart is imaged after the administration of radiopharmaceuticals labeled with radionuclides having different primary photon energies. Finally, small-animal SPECT and

SPECT/CT systems are rapidly advancing, facilitating the performance of myocardial metabolic studies in rodent models of cardiac disease.

Several fatty acid imaging tracers have been developed for clinical imaging with SPECT. These include radioiodinated straight long-chain fatty acids, including 15-(*p*-iodophenyl) pentadecanoic acid and branched fatty acids, such as ^{123}I-β-methyl-*p*-iodophenyl-pentadecanoic acid (BMIPP). Straight long-chain fatty acids enter the mitochondria and are metabolized by β-oxidation immediately, whereas BMIPP is not initially metabolized via β-oxidation because the methyl substitution precludes the formation of the ketoacyl coenzyme A intermediate. The prolonged retention of BMIPP in the cardiomyocyte is suitable for a longer acquisition time that is necessary for SPECT. Similar to ^{18}F, ^{123}I is cyclotron-produced but with a longer half-life of 13 h. The longer half-life of ^{123}I facilitates centralized distribution of the radiotracer, as with a conventional radiopharmaceutical. No specific SPECT radiotracers are currently available to measure myocardial glucose metabolism. However, when combined with the appropriate detection scheme or collimator design, myocardial glucose metabolism can be measured with SPECT and ^{18}F-FDG (*2*). The major disadvantage of SPECT is its inability to quantify cellular metabolic processes of interest. This limitation is primarily caused by the technical limitations of SPECT—relatively poor temporal and spatial resolution—and the limited metabolic information provided by the kinetics of the SPECT radiotracers.

PET

Noninvasive measurement of myocardial metabolism is most commonly performed with PET because of its intrinsic quantitative capability and the use of radiopharmaceuticals labeled with the positron-emitting radionuclides. The PET detection scheme permits both the accurate quantification of activity in the field of view and its temporal distribution. These 2 pieces of information are critical to quantifying metabolic processes of interest. The positron-emitting radionuclides of the biologically ubiquitous elements oxygen (^{15}O), carbon (^{11}C), and nitrogen (^{13}N), as well as fluorine (^{18}F) substituting for hydrogen, can be incorporated into a wide variety of metabolic radiotracers that participate in a variety of biochemical pathways without altering the biochemical properties of the substrate of interest (Table 1 in the preceding review by Taegtmeyer (*1*)). By analyzing different components of the tracer kinetic curves (e.g., uptake, fast washout, and slow washout) with appropriate and well-validated mathematic models, it is possible to quantify specific metabolic processes. Examples include the quantification of myocardial oxygen consumption, fatty acid uptake, oxidation and esterification, glucose uptake, glycolysis and oxidation, and lactate oxidation (*3–5*). As with SPECT, small-animal PET and PET/CT systems have been developed that permit measurements of myocardial metabolism in the rodent heart similar to those done in the human heart. Despite its strengths, PET has several limitations that hinder its broader applicability to measure myocardial metabolism. These include the high cost of the PET systems, the need for an on-site cyclotron and expertise in radiopharmaceutical synthesis (except for ^{18}F-FDG), and the relative complexity of the image quantification schemes.

MRS

MRS of the heart is a powerful research tool. Its use offers great advantages for metabolic evaluation of whole organs by providing unique, chemically specific information on true metabolic flux rates through pathways and specific enzymes, content and turnover of key metabolite pools, and transport kinetics across membranes. MRS of the whole heart has proven valuable for the evaluation of the energetic state and energy substrate use by the heart, such as carbohydrate versus fatty acid use (*6–8*). The dynamic processes described previously, uniquely accessible by MRS, provide unique mechanistic insight linking metabolic derangements to the contractile dysfunctions that are associated with various cardiac disorders, such as myocardial ischemia, reperfusion, and hypertrophy (*9,10*). Moreover, MRS enables detection of endogenous, nuclear MR (NMR)–sensitive metabolites (nuclei possessing net spin, $I \geq 1/2$), such as compounds containing ^{31}P and ^{23}Na (*6,7*). Recent advances in the applications of localized detection of NMR signals, or MRS, from selected regions of interest in the in vivo heart of animal models and humans have also expanded the applicability of assessing cardiac metabolism for clinical evaluations and in vivo heart models of disease in animals.

However, MRS is not without limitations, the most notable being the relative insensitivity of the approach because of low signal-to-noise ratio (SNR) compared with radionuclide approaches for metabolic evaluation. The insensitivity of the technique requires the administration of exogenous metabolic precursors, labeled with NMR-detectable nuclei, in millimolar concentrations as opposed to radiotracer methods that typically use nanomolar and picomolar concentrations. In addition, the physics of NMR detection schemes for a deep structure such as the heart present unique challenges because of the potential for heating of tissue secondary to the application of the radiofrequency energy necessary to produce the MR signal (e.g., specific absorption rate). Nevertheless, the chemical specificity of MRS makes this approach highly complementary to radionuclide studies of spatial distribution, uptake, and clearance of radiolabeled metabolic precursors. A fundamental advantage of information from MRS of the heart is that the signals of interest emanate from intracellular metabolites, which can even be distinguished, in some circumstances, from extracellular pools.

APPLICATION OF SPECT

SPECT of Glucose Metabolism

The perfusion–metabolism mismatch pattern on ^{18}F-FDG PET is the reference standard for detecting reversible left

ventricular dysfunction in the clinical setting. ^{18}F-FDG PET has proven benefit for the recovery of function, for improvement in detecting heart failure symptoms, and for predicting survival after revascularization (*11–14*). SPECT metabolic imaging with either ^{201}Tl or ^{99m}Tc tracers is also reliable in detecting myocardial viability, particularly in patients with mild to moderately impaired left ventricular dysfunction (left ventricular ejection fraction of 25%−50%) (*15–17*).

Advances in high-energy collimation SPECT cameras have made imaging of positron emitting tracers, such as ^{18}F, possible. Moreover, ^{18}F-FDG metabolic imaging using SPECT equipped with a high-energy collimator simultaneously with a SPECT perfusion agent has the additional advantage of acquiring myocardial perfusion data. Studies have shown that when SPECT flow tracers such as ^{99m}Tc-sestamibi or ^{201}Tl are used in combination with ^{18}F-FDG SPECT, the detection of myocardial viability is similar to that with PET (*18–20*). However, the poorer spatial resolution of SPECT, its lower sensitivity, and the lack of attenuation correction may cause some discordance between images of the same tracer measured with SPECT and PET (*17,21*). Given these technical limitations of ^{18}F-FDG SPECT, in addition to the limited number of publications on a small number of subjects, this technique has not received approval from the Food and Drug Administration or the Centers for Medicare and Medicaid Services for imaging the heart in the clinical setting.

Beyond its proven value for myocardial viability, the metabolic signature of reduced fatty acid metabolism and increased glucose use may serve as a sensitive marker of myocardial ischemia (*22,23*). Indeed, this metabolic signature may persist well after the resolution of the inciting ischemic event; this persistence has been termed ischemic memory (*24,25*). Applying a dual-isotope sestamibi and ^{18}F-FDG simultaneous injection and acquisition protocol, this metabolic switch from fatty acid to glucose was recently shown to occur promptly when myocardial ischemia is induced during exercise and to persist for up to 24 h despite normal perfusion under resting conditions (Fig. 1) (*2,26*). Similarly, decreases in regional fatty acid metabolism and delayed recovery of fatty acid metabolism, long after regional blood flow has returned to baseline, have been shown when using BMIPP. Taken in sum, these studies show that ischemic memory occurs in humans and can be imaged with conventional radionuclide approaches, raising the potential for using these techniques in managing patients with ischemic heart disease.

Although the technical limitations of a modified SPECT camera to detect ^{18}F signals over PET are well recognized, other challenges also exist for acquiring ^{18}F-FDG studies with either SPECT or PET. For example, studies to detect myocardial ischemia are typically performed under fasting conditions to maximize the differences in tracer uptake between ischemic myocardium (increased uptake) and nonischemic tissue (reduced uptake). However, under fasting conditions, there is heterogeneous distribution of ^{18}F-FDG in the myocardium even in healthy subjects, which creates another level of complexity in image interpretation (*27*). Thus, when it comes to the cardiac application of ^{18}F-FDG to detect myocardial ischemia under fasting conditions, it may be difficult to resolve and conclusively localize the hotspot ^{18}F-FDG signal in the ischemic myocardium when the rest of the myocardial regions have no discernable signal to serve as a reference standard. Such studies will require either simultaneous acquisition of myocardial perfusion or hybrid SPECT/CT with anatomic coregistration of the heart.

SPECT of Fatty Acid Metabolism

As mentioned previously, measurement of myocardial fatty acid metabolism using BMIPP is the most commonly

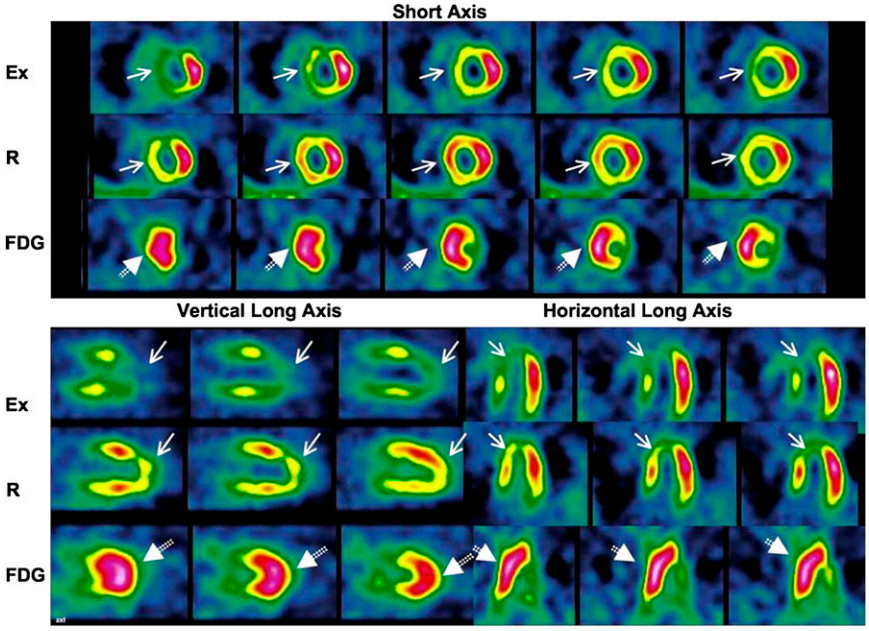

FIGURE 1. Simultaneous myocardial perfusion and metabolism imaging after dual intravenous injection of ^{99m}Tc sestamibi and ^{18}F-FDG at peak exercise (Ex). Dual-isotope simultaneous acquisition was performed 40–60 min after exercise study was completed. Rest ^{99m}Tc-sestamibi imaging (R) was performed separately. In this patient with angina and no prior myocardial infarction, note evidence of extensive reversible perfusion defect in anterior, septal, and apical regions. Coronary angiogram showed 90% stenosis of left anterior descending and 60% of left circumflex coronary arteries. Corresponding ^{18}F-FDG image shows intense uptake in regions with reversible sestamibi defects reflecting metabolic correlate of exercise-induced myocardial ischemia. (Adapted from (*2*).)

used metabolic application of cardiac SPECT. Similar to ^{18}F-FDG, BMIPP is taken up by the myocyte but is not further metabolized after the first step in this metabolic pathway. After a transient ischemic event, defects in fatty acid metabolism, as assessed by BMIPP distribution, are present in patients undergoing exercise myocardial perfusion SPECT studies (Fig. 2), as well as in patients presenting with acute coronary syndromes (*22,23*). This long-duration disturbance in metabolism is similar to that seen after ^{18}F-FDG administration.

Uptake of BMIPP from the plasma into myocardial cells occurs via the CD36 transporter protein present on the sarcolemmal membrane. Once BMIPP is taken up by the myocyte, it undergoes adenosine triphosphate (ATP)–dependent thioesterification but does not undergo significant mitochondrial β-oxidation. Retention of BMIPP in the intracellular lipid pool of the myocardium most likely reflects activation of fatty acids by coenzyme A, and indirectly, of cellular ATP production resulting from fatty acid metabolism. Thus, in the setting of myocardial ischemia, reduction in ATP production secondary to diminished fatty acid metabolism is mirrored by decreased myocardial BMIPP uptake. Important clinical applications of the latter are the early assessment of chest pain among patients presenting to the emergency department with acute coronary syndromes and the assessment of myocardium at risk among patients presenting with acute myocardial infarction and early reperfusion with either percutaneous intervention or thrombolysis. Results from a recent multicenter clinical trial suggest that the combination of BMIPP SPECT with initial clinical information results in improved sensitivity for identifying patients with acute coronary syndrome compared with the sensitivity of the initial clinical diagnosis alone, while at the same time maintaining specificity (*28*).

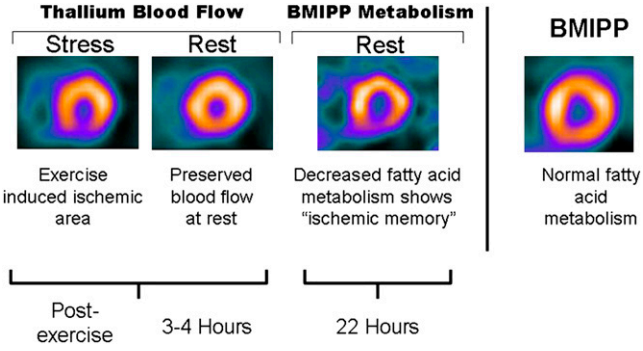

FIGURE 2. SPECT image shows delayed recovery of regional fatty acid metabolism after transient exercise-induced ischemia, termed ischemic memory. Representative stress (left) and rest reinjection (second from left) short-axis thallium tomograms demonstrate reversible inferior defect consistent with exercise-induced myocardial ischemia. After injection of BMIPP, labeled tomogram (second from right) acquired at rest 22 h after exercise-induced ischemia shows persistent metabolic abnormality in inferior region despite complete recovery of regional perfusion at rest, as evidenced by thallium reinjection image. Tomogram on far right shows retention of BMIPP in heart of healthy adult for comparison. (Adapted from (*25*).)

The deleterious effect of altered myocardial metabolism was recently also demonstrated in patients with end-stage renal disease (*29,30*). A shift in myocardial metabolism from fatty acid to glucose may contribute to the cardiomyopathic process observed in late-stage kidney disease (*30*). The cardiomyopathy typical of chronic kidney disease and the associated uremia are thought to lead to a myocytes–capillary mismatch, with a diminished vascular supply relative to the number and volume of functioning myocytes (*31*). The oxygen-poor milieu leads to diffuse myocardial ischemia with an anticipated decline in aerobic myocardial fatty acid use. Such altered cardiac metabolism, indicating silent myocardial ischemia, was recently shown to be highly prevalent among asymptomatic dialysis patients with no history of myocardial infarction, and was able to identify the subgroup of patients who were at high risk of cardiac death (*30*).

Future Directions and Challenges

SPECT of myocardial metabolism has focused primarily on the concept of ischemic memory. Delayed recovery of fatty acid metabolism detected with SPECT up to 30 h after the resolution of transient myocardial ischemia provides the potential for diagnosing antecedent myocardial ischemia both in the chronic and in the acute setting. As a consequence, targeting intracellular fatty acid metabolism with SPECT may expand our ability to diagnose and treat subclinical myocardial ischemia or progressive cardiomyopathy (e.g., chronic kidney disease) that often remains elusive with traditional imaging approaches. However, to achieve these goals, several hurdles must be overcome. From a technical perspective, imaging protocols need to be optimized with respect to timing of imaging after chest pain, acquisition schemes that account for ^{123}I need to be standardized, and questions regarding the need to standardize the substrate environment must be resolved. From a clinical point of view, the diagnostic and prognostic accuracy and the added clinical information provided by these metabolic signatures need to be determined.

APPLICATION OF PET

^{18}F-FDG PET

As mentioned previously, myocardial viability imaging using ^{18}F-FDG has emerged as a highly valuable clinical tool. As molecular imaging evolves, seeking tools that could be translated to clinical practice, it is worthwhile to examine ^{18}F-FDG and what has led to its success as a probe—namely, more than 30 y of experience (*32*), straightforward production and imaging, wide availability, high accuracy, linkage to disease and outcomes, and impact on patient management (Fig. 3). ^{18}F-FDG PET is the most sensitive viability method for predicting wall motion

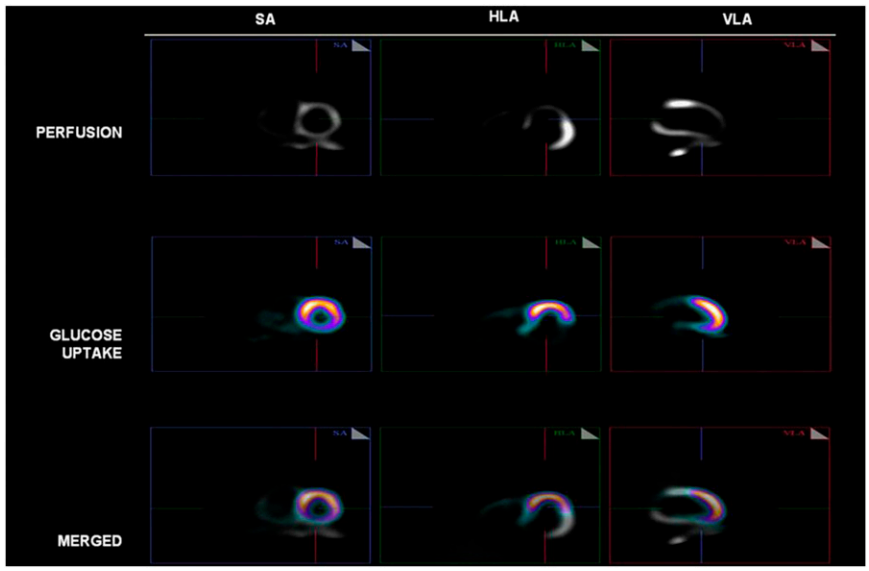

FIGURE 3. Example of hibernating myocardium. Images show moderate perfusion defect involving apex and mid to distal anterior and septal walls (superior row) but preserved ^{18}F-FDG uptake, which allows delineation of hibernating myocardium in distribution of territory of left anterior descending artery (inferior row). SA = short axis, HLA = horizontal long axis, VLA = vertical long axis.

recovery (*33*) and identifies patients at increased risk for death if they do not undergo revascularization. The PET and Recovery Following Revascularization (PARR-2) trial showed a trend for benefit when ^{18}F-FDG PET was used to assist management (*34*). In patients who adhered to recommendations, significant outcome benefits were attained, with the degree of hibernation predicting the likelihood of response to revascularization (*35*). A post hoc subgroup analysis demonstrated improved outcomes in an experienced center (*36*). As a consequence, regional networks that work to ensure quality and clinical expertise at different ^{18}F-FDG PET sites are now being established (*37*).

Phenotype Characterization and Translational Imaging

Quantitative measurements of myocardial metabolism are now possible in the rodent heart using small-animal PET. For example, measurements of myocardial glucose uptake using small-animal PET have been shown to relate to the protein expression of the glucose transporter-4 protein levels (*38*). Moreover, small-animal PET has helped clarify the mechanisms responsible for the metabolic alterations that occur in various diseases. For example, in mice with cardiac-restricted overexpression of the nuclear receptor, peroxisome proliferator-activated receptor α-(PPARα), a key regulator of myocardial fatty acid uptake, oxidation, and storage, demonstrates a metabolic phenotype that is similar to that in diabetic hearts (*39*). Small-animal PET studies with ^{11}C-palmitate and ^{18}F-FDG in mice demonstrate an increase in fatty acid uptake and oxidation and an abnormal suppression of glucose uptake. In contrast, in mice with cardiac-restricted overexpression of PPARβ/δ, small-animal PET measurements showed an increase in glucose uptake and reduced fatty acid uptake and oxidation (Fig. 4) (*40*). Taken in sum, these observations show that PPARα and PPARβ/δ drive different metabolic regulatory programs in the heart and that imaging can help characterize genetic manipulations in the mouse heart. These observations highlight the importance of small-animal PET to evaluate phenotype and transgene expression. However, small-animal PET has to overcome several challenges in imaging the rodent heart, including partial-volume effects, extraction of the input function for quantification, and other technical factors. Thus, reproducing in the rodent setting the success observed in humans can be a challenge.

To further translate metabolic imaging in the clinical field, the myocardial metabolic phenotype in experimental models of disease should be also applicable in humans. One such example is the *PRKAG2* cardiac syndrome, which is characterized by arrhythmias and hypertrophy caused by a mutation in the *PRKAG2* gene that codes for adenosine monophosphate–activated protein kinase (AMPK), a key metabolic regulator in the myocyte (*41*). The central role of AMPK in regulating glucose metabolism had led to the hypothesis that the pathologic basis of the *PRKAG2* cardiac syndrome was caused by impaired glucose metabolism and excessive glycogen storage (*42*). Indeed, patients and the corresponding transgenic mouse model are characterized by increased glycogen storage. Preliminary data in the transgenic model show reduced ^{18}F-FDG uptake that can be quantified (Fig. 5) (*43*). Recently, human studies demonstrated reduced ^{18}F-FDG uptake (*44*). At first blush, the lower level of glucose uptake appears paradoxical because cardiac hypertrophy caused by excessive glycogen storage is a hallmark of this condition. This apparent paradox may be explained by the developing nature of the disease process and highlights the potential importance of serial imaging to better characterize the time course of the disease. In another example, altered fatty acid and oxidative metabolism were shown in a group of patients with mutation in the α-tropomyosin gene and associated left

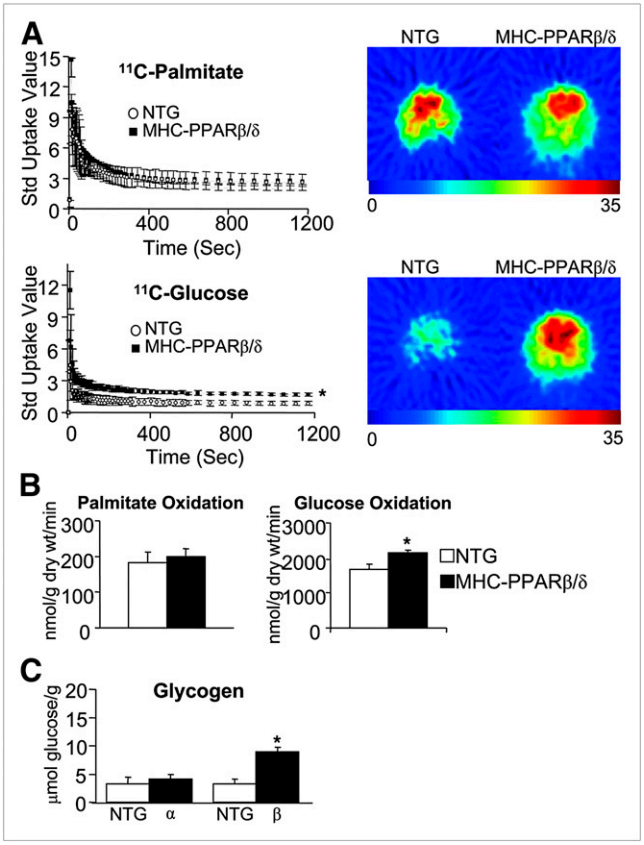

FIGURE 4. Increased myocardial glucose use in myosin heavy chain (MHC)-PPARβ/δ mice. (A) On left, standardized uptake value time–activity curves for ^{11}C-palmitate and ^{11}C-glucose into female MHC-PPARβ/δ–high-expression (HE) and nontransgenic (NTG) hearts as determined by small-animal PET. On right, representative small-animal PET images at 20 s after tracer injection. Images are normalized to total amount of radioactivity injected and body weight. Relative amounts of tracer uptake are indicated by color scale. (B) Oxidation of palmitate and glucose was assessed in isolated working hearts of 12-wk-old male MHC-PPARβ/δ-HE and NTG control mice. Bars represent mean oxidation rates expressed as nanomoles of substrate oxidized per gram of dry mass per minute. (C) Glycogen levels were assessed in mouse hearts from male MHC-PPARα–low-expression and MHCPPARβ/δ-HE mice and NTG controls. Results are presented as glucose released from glycogen and normalized to tissue weight. *$P < 0.05$ vs. NTG. (Reprinted with permission of (*40*).)

ventricular hypertrophy (*45*). Taken together, these data highlight the advances in small-animal PET technology to quantify metabolic parameters and exemplify the translational capabilities of metabolic PET.

Future Directions and Challenges

Several promising developments augur well for the continued need for metabolic imaging with PET. Clinical research studies are exploring new roles for metabolic imaging in the diabetic heart, myocardial hypertrophy, and ischemic memory. The emergence of new drugs that target specific metabolic processes, such as fatty acid oxidation (e.g., PPARα and PPARβ/δ agonists) or insulin sensitivity (glucagon-like peptide-1), is creating a need to direct and monitor metabolic response, paving a path for personalized therapy directed by metabolic imaging.

Metabolic imaging works well as a clinical tool in the context of viability imaging, but metabolic alterations in nonischemic disorders are common and not well understood. Imaging tools are available to enhance metabolic phenotype characterization, and translation to humans is possible. However, comparative effectiveness research is needed to understand the clinical value of metabolic imaging and how it compares with other emerging methodologies.

APPLICATION OF MRS

Myocardial Energetics

^{31}P NMR has long been used to assess high-energy phosphate content in the intact beating heart. Indeed, the earliest clinical studies with cardiac MRS provided evaluations of the myocardial energetic state from the relative contents of high-energy phosphates via ^{31}P detection (*46–48*). Cardiac ^{31}P MRS in patients provides information on the relative contents of phosphocreatine (PCr) and ATP (*46–50*). A widely used parameter for assessing the relative energy state of the heart has been the ratio of PCr to ATP content, as detected by ^{31}P MRS, and this approach was instrumental in showing the now well-recognized impaired energetic state of the failing heart.

The diseased myocardium shows a generally reduced PCr-to-ATP ratio, but one limitation of the parameter for clinical use is the lack of specificity. Reduced PCr-to-ATP is generally evident in patients with either hypertrophic or dilated cardiomyopathies, allograft rejection after cardiac transplantation, or coronary artery disease with stenosis (*48–51*). Fortunately, important new advances in ^{31}P MRS detection extend well beyond the original uncertainties of the pathophysiologic specificity of the PCr-to-ATP ratio of the heart. One such example is the use of MRS magnetic transfer techniques to measure the activity of the creatine kinase system, which provides a balance between energy production, transport, and use. Indeed, application of this approach in clinical subjects suggests better delineation of failing from nonfailing, hypertrophic hearts when compared with the PCr-to-ATP ratio (Figs. 6 and 7) (*52*).

Although ^{31}P MRS provides unique information on the energetic state of the myocardium, the underlying mechanisms of energy production pathways via the intermediary metabolism can be detected by exploiting stable isotope kinetics. Naturally abundant at only 1.1%, the nonemitting ^{13}C is well suited for enrichment studies of metabolism and is commonly used for in vitro analysis of the fractional contributions of carbon-based substrates for oxidative production of ATP, as determined by ^{13}C isotopomer distributions in the glutamate pool of tissue

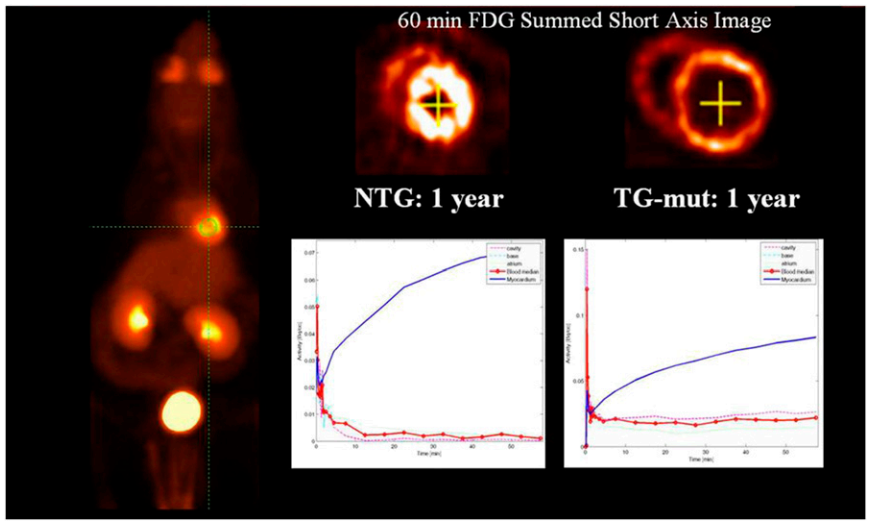

FIGURE 5. On left, cardiac imaging in mouse model. On right, short-axis display of ^{18}F-FDG myocardial uptake (60 min) in NTG and transgenic-mutant (TG-mut) of *PRKAG2* gene. Note that ^{18}F-FDG uptake in NTG is normal, whereas in transgenic-mutant it is significantly reduced. Below, graphs show arterial blood (red) and myocardial (blue) time–activity curves. In transgenic-mutant, myocardial curve shows lower rate of ^{18}F-FDG uptake compared with that in NTG. (Courtesy of M.H. Gollob and S. Thorn.)

extracts (*53,54*). ^{13}C detection of enrichment rates in metabolites provides the basis for understanding metabolic flux regulation and the metabolic support of contractile function through shifts in enzyme isoform expression in normal and diseased hearts. After the introduction of ^{13}C-enriched precursors to the heart, such as glucose or fatty acids, the enrichment rates of targeted metabolites can be monitored sequentially for kinetic analysis either in isolated perfused hearts or in vivo (*8,10,55*). For example, NMR spectra can be obtained from the beating heart to monitor rates of palmitate oxidation or storage into triacylgyceride (Fig. 8). Recent applications for ^{13}C MRS in experimental animal models enable measurement of metabolic enzyme activity caused by altered gene expression in the intact functioning heart (*10,55*).

Dynamic-mode ^{13}C MRS has provided a mechanistic understanding of enzyme isoform changes, and even mitochondrial transport function, in isolated organs and animal models of heart disease (*10,55,56*). The use of ^{13}C-enriched long-chain fatty acids in isolated rat and mouse heart perfusion studies has enabled comparison of the rates of fatty acid oxidation by mitochondria and storage in the triacylglyceride pool, providing a comprehensive view of lipid dynamics in normal and diseased hearts (*57–59*). For example, ^{13}C MRS of hypertrophied rat hearts, isolated and perfused with the long-chain fatty acid, palmitate, that is ^{13}C-enriched at novel carbon-chain sites, has shown reduced rates of long-chain fatty acid oxidation and impaired turnover in the triacylglyceride pool (*10,59*). The reduced fat oxidation coincides with the apparent compensatory recruitment of an alternate mode of carbohydrate entry into oxidative pathways, via anaplerosis, through upregulation of malic enzyme expression in hypertrophied hearts (*10,60*). Pharmacologic reversal of this up-regulated anaplerotic activity in cardiac hypertrophy produced a surprising increase in contractility of the hypertrophied rat heart (*60*). These findings show how such basic evaluations of experimental models with MRS contribute to elucidating links between metabolic flux in the intact beating heart and contractile performance. These links hold obvious relevance for the development of potential therapeutic, metabolic protocols that combat contractile dysfunction in the diseased heart.

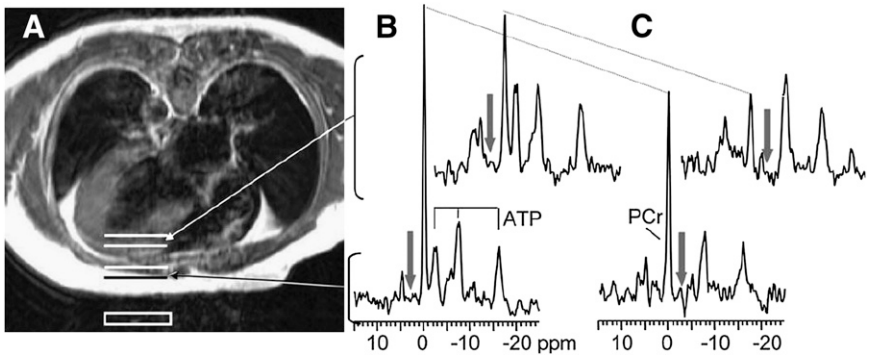

FIGURE 6. (A) Axial MR image of patient with left ventricular hypertrophy and congestive heart failure in which region of localized ^{31}P NMR spectra from chest and left ventricle are identified (rectangular outline). (B) ^{31}P NMR spectra from chest muscle (bottom) and left ventricle (top) with control saturating radiofrequency irradiation (arrow). (C) ^{31}P NMR spectra from chest muscle (bottom) and left ventricle (top) with selective, saturating radiofrequency irradiation at γ-phosphate resonance (arrow). Note decreased magnitude of PCr signal in panel C due to chemical exchange with saturated ^{31}P nuclei of γ-phosphate of ATP. Decreased PCr signal depends on rate of ATP synthesis through creatine kinase reaction (*52*).

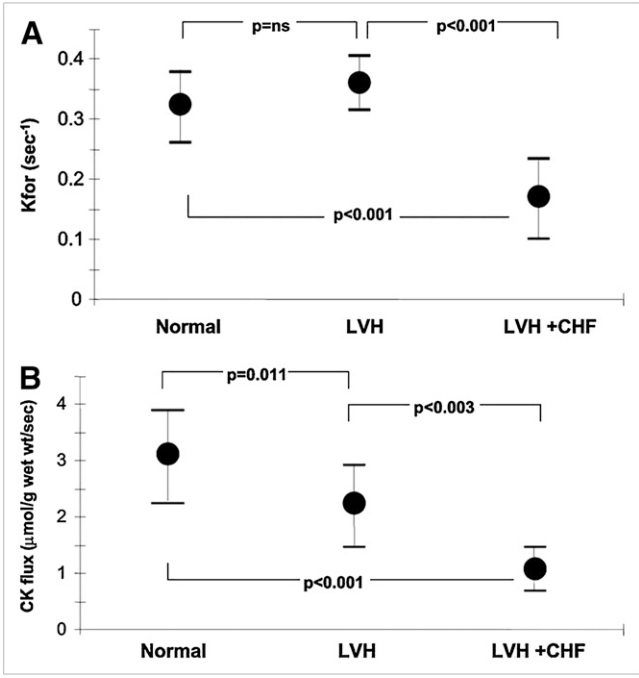

FIGURE 7. (A) Pseudo first-order rate constant (K_{for}) for creatine kinase (CK) in hearts of healthy subjects (Normal), patients with left ventricular hypertrophy (LVH), and patients with LVH and congestive heart failure (LVH + CHF). (B) ATP flux through CK in each group. Note depressed flux rate in LVH + CHF. (Reprinted with permission of (*52*).) ns = not significant.

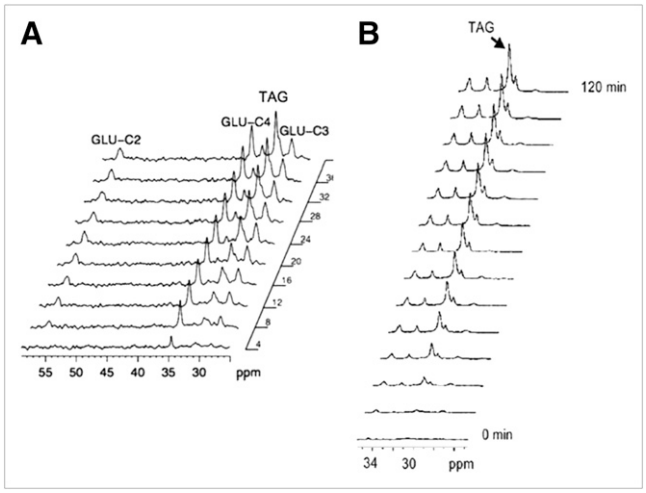

FIGURE 8. (A) Sequential ^{13}C NMR spectra (2 min each) of isolated rat heart oxidizing ^{13}C-enriched palmitate. Relative rates of isotope enrichment of glutamate 2-, 3-, and 4-carbons (GLU C-2, GLU C-3, GLU C-4, respectively) provide measures of oxidative rates. Progressive enrichment of triacylglyceride (TAG) provides TAG turnover. (B) Selected ^{13}C NMR spectra (2 min each) of isolated mouse heart, perfused with ^{13}C palmitate, show progressive enrichment of TAG for measures of TAG turnover in transgenic models.

Just as important, whereas ^{13}C MRS has enabled detection of increased anaplerosis in hypertrophied hearts, experimental evaluation of metabolism with radioactive ^{14}C and release rates of $^{14}CO_2$ from oxidation of ^{14}C-labeled precursors are insensitive to the detection of anaplerotic mechanisms. $^{14}CO_2$ release methods, when used alone, do not detect changes in CO_2 fixation into the citric acid cycle intermediate pools that are associated with anaplerotic reactions, and consequently may lead to an overestimation of mismatches between the rates of glycolysis and glucose oxidation. Thus, despite the limitation of nontracer levels of exogenous materials, ^{13}C MRS studies have already offered unique perspectives not previously accessible by other labeling methods.

Although the examples discussed previously demonstrate a unique role for ^{13}C studies of the intact heart, the requirements for a second resonance frequency for proton decoupling of these ^{13}C NMR spectra and the limited sensitivity of ^{13}C MRS detection present significant physical limitations for noninvasive in vivo applications. Therefore, the recent use of hyperpolarization of ^{13}C in specific compounds to provide 10,000- to 20,000-fold increases in SNR holds great potential. The use of dynamic nuclear polarization to hyperpolarize ^{13}C has already enabled high SNR detection for animal studies on isolated hearts and rapid temporal resolution for in vivo rat heart studies (Fig. 9) (*61–63*). With dynamic nuclear polarization, the hyperpolarized state of the ^{13}C nuclei lasts for approximately 1 min, which is sufficient time for injection and collection of in vivo MRS data in serial fashion, with acquisition intervals of sequential spectra on the order of seconds (Fig. 9) (*62,63*). Although current in vivo studies with hyperpolarized ^{13}C rely on detection after bolus intravenous injections of ^{13}C-enriched precursors at relatively large, millimolar concentrations, the increase in SNR holds the potential for the eventual development of studies using tracer levels that would not influence the metabolic pathways of interest. At present, chemistry of the dynamic nuclear polarization excitation limits the availability of relevant precursor molecules that enable practical durations of the nuclear hyperpolarization for delivery and detection by MRS. For this reason, ^{13}C hyperpolarization studies in hearts have been limited to the fate of pyruvate. However, increased development in the chemistry of these hyperpolarized nuclei in other precursors offers the promise for a more comprehensive application of hyperpolarized ^{13}C NMR and MRS for in vivo cardiac metabolism.

Proton (^1H) MRS is more accessible to current in vivo and clinical studies. Localized ^1H MRS, of both animal models and human subjects, offers unique evaluation of lipid infiltration of internal organs (*64,65*). In the heart, ^1H detection provides quantitative analysis of the intramyocardial mobile lipid from methylene group protons (CH_2) in acyl chains generally associated with triacylglyceride. Notably, such evaluation relies on ^1H signal, which is localized from the left ventricular septum, to eliminate

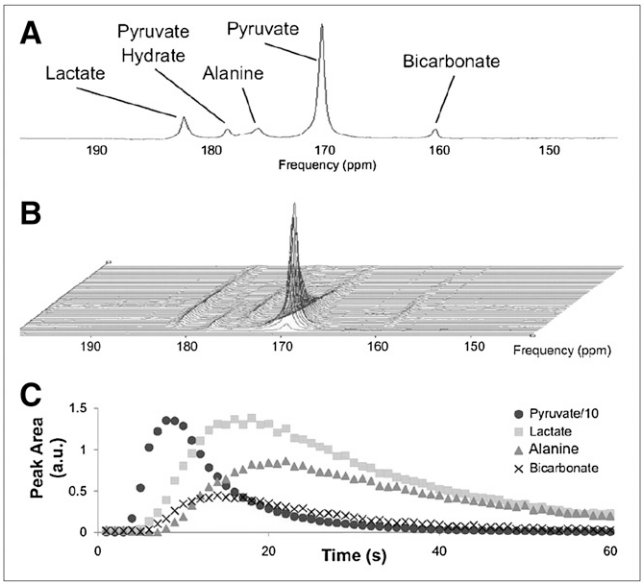

FIGURE 9. In vivo ^{13}C NMR spectra from heart of anesthetized rat after bolus tail vein injection of 1 mL of 80 mM sodium [1-^{13}C] pyruvate. (A) Spectrum displaying ^{13}C-enriched metabolites of pyruvate. (B) Sequential spectra acquired every second for 1 min after injection. (C) Time course of signals from pyruvate (solid circle), lactate (square), alanine (triangle), and bicarbonate (X). a.u. = arbitrary units. (Reprinted with permission of (*62*).)

contaminating signal from the pericardial fat that is adjacent to the free wall. Increased intramyocardial lipid, as identified by ^1H MRS, may be linked to lipotoxic effects that impair cardiomyocyte function and has been associated with the development of diabetic cardiomyopathy. For example, the presence of increased myocardial lipid detected by ^1H MRS has been shown in diabetics and appears to be associated with a decline in diastolic function (*64,66*). Moreover, a prolonged caloric restriction in obese diabetic patients and its attendant salutary effect of glucoregulation decreases myocardial lipid and improves diastolic function (*67*). Thus, it appears that myocardial lipid levels may have a detrimental effect on diastolic function in diabetes and that lipid levels are responsive to changes in plasma fatty acid delivery. As interest mounts in monitoring lipid accumulation in the heart, the advantages of high- and ultrahigh-field magnet systems become increasingly apparent. The advantageous improvements in SNR with high field strength are apparent in the comparison of in vivo lipid signals from ^1H MRS of in vivo hearts, at the clinical field of 1.5 T and from a research magnet at 14.1 T, as shown in Figures 10 and 11, respectively.

Preliminary results suggest that MRS of myocardial lipid content can be combined with high-resolution cardiac tagging MRI at 14.1 T for a comprehensive study combining metabolic evaluation with transmural measures of compression and stretch, via 2-dimensional principle strains (E1 and E2) across the left ventricular wall (*68*). This work indicates that intramyocardial lipid infiltration increases myocardial stiffness, as evidenced by reduced endocardial compression and stretch in the left ventricular wall.

Future Directions and Challenges

The specific examples highlighted here show an array of cardiac applications for NMR spectroscopy and MRS. Although some schemes hold diagnostic value for direct clinical evaluation, others provide basic information to elucidate mechanisms of contractile dysfunction and contribute to the development of therapeutic strategies for heart disease. Although the technical challenges presented by some of the more sophisticated methods for kinetic analysis limit current applications to experimental heart models, the chemically specific nature of MRS provides a valuable correlate to clinical evaluations with nuclear modalities such as PET and SPECT. Combining metabolic evaluation by MRS with functional assessment by MRI is emerging as a powerful combination.

APPLICATION OF ULTRASOUND

Ultrasound, Targeted Contrast Agents, and Ischemic Memory

Although ultrasound has not been used to measure specific myocardial metabolic processes, it can be used to

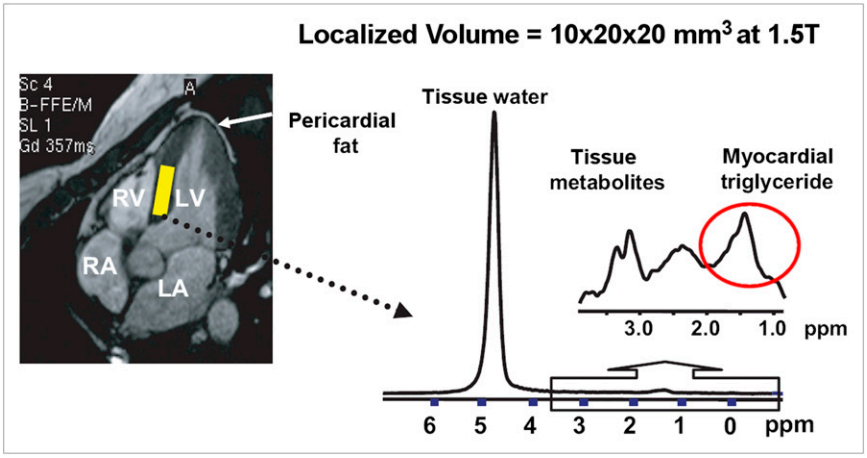

FIGURE 10. Localized ^1H MRS signal from myocardial triacylglyceride in human. Left panel shows MR image of heart displaying localized volume in left ventricular (LV) septum for MRS (yellow rectangle). Right panel displays ^1H NMR spectrum with inset of expanded region of triacylglyceride signal (in red circle). (Adapted with permission of (*64*).) RV = right ventricle; RA = right atrium; LA = left atrium.

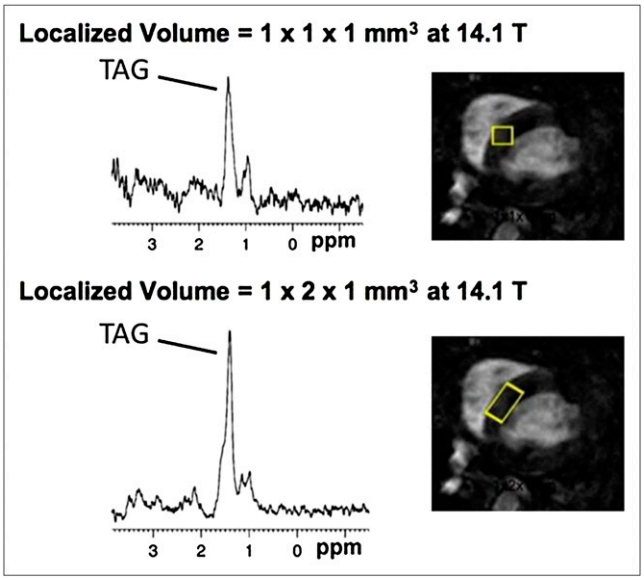

FIGURE 11. Localized ^{1}H MRS signals from myocardial triacylglyceride (TAG) of in vivo anesthetized mouse heart at 14 T with localized volume of left ventricular septum for MRS indicated at right in axial MR image of heart (yellow box). Top panel displays signals from triacylglyceride within a $1 \times 1 \times 1$ mm voxel. Bottom panel displays enhanced signal from increased voxel size of $1 \times 2 \times 1$ mm. (Courtesy of E. Douglas Lewandowski.)

detect cellular signatures of antecedent myocardial ischemia. As mentioned previously, transient myocardial ischemia results in reduced fatty acid metabolism and increased glucose metabolism that persist after the resolution of the ischemia, leading to the concept of ischemic memory. These metabolic signatures can be detected with either SPECT or PET as a means to indicate an antecedent ischemic event. Another approach to imaging recent myocardial ischemia is to target the stereotypical inflammatory response to an ischemic insult. This is characterized by sequential microvascular endothelial overexpression of leukocyte adhesion molecules that mediate leukocyte slowing, rolling, capture, and firm adhesion to the endothelium (*69–71*). On ischemic insult, the leukocyte adhesion molecule P-selectin is rapidly mobilized to the endothelial surface from preformed cytoplasmic stores within minutes of ischemia and reperfusion, where it mediates transient tethering interactions that result in leukocytes rolling along the endothelium (*71*). Leukocyte rolling enables leukocyte interaction with adhesion molecules such as intercellular adhesion molecule-1 (ICAM1) or vascular adhesion molecule (VCAM), which mediate firm attachment (*69*). Unlike preformed cytoplasmic P-selectin, which mobilizes quickly to the surface of endothelium on ischemia and reperfusion, postischemic expression of ICAM and VCAM is transcriptionally dependent, requiring several hours to manifest after ischemic insult. Because adhesion molecule expression and leukocyte adhesion are endothelial events, an imaging probe that remains in the intravascular space, such as an ultrasound contrast agent, could be adapted to detect these hallmarks of inflammation.

Ultrasound contrast agents are gas-filled microspheres (microbubbles) used in ultrasound imaging for acoustically opacifying the blood pool. The microbubbles, ranging from 1 to 4 μm in diameter, are typically perfluorocarbon- or nitrogen-gas microspheres encapsulated by shells of varying composition, such as phospholipids, albumin, or biodegradable polymers (*72*). Because of their size and shell composition, the microbubbles do not interact with the endothelium and transit in unimpeded fashion through the microcirculation (*73*). In the presence of an ultrasound field tuned to the appropriate frequency and acoustic pressure, the microbubbles expand and contract (oscillate) in a nonlinear fashion, themselves becoming emitters of ultrasound that can be detected and displayed as a transient signal on a 2-dimensional ultrasound image (*74*). This acoustic property has been the basis for the use of microbubbles as red cell tracers in applications such as enhancement of the blood pool for endocardial border detection in technically difficult echocardiograms and myocardial perfusion imaging (*75–78*).

For ultrasound molecular imaging applications, targeting ligands are conjugated to the microbubble shell, conferring the ability of a microbubble to attach to a specific endothelial epitope, resulting in persistent ultrasound contrast enhancement and hence the capability for investigating the endothelial phenotype (*79*). The surface of microbubbles has been conjugated to a variety of targeting ligands, including monoclonal antibodies, peptides, and naturally occurring protein and carbohydrate ligands, for the in vivo acoustic detection of inflammation and angiogenesis in animal models of cardiac and noncardiac disease (Fig. 12A) (*79–83*). Alternatively, a nonligand-based approach for imaging inflammation has also been described, in which activated leukocytes adhering to the endothelium are rendered acoustically active by lipid microbubbles that attach to the leukocyte surface through a process that is thought to be complement-mediated (Fig. 12B) (*84–86*).

Based on these considerations, it has been possible to acoustically detect antecedent ischemia using ultrasound contrast agents designed to bind to inflammatory endothelium. The rapidity with which P-selectin is expressed after ischemia and reperfusion makes it an attractive marker when the clinical dilemma is to determine whether myocardial ischemia has recently occurred. Furthermore, its location on the endothelial cell surface renders it accessible to an intravascular probe such as a microbubble.

The concept of P-selectin targeting by a microbubble was first proven in a murine model of renal ischemia and reperfusion. Monoclonal antibody to P-selectin was conjugated to a lipid microbubble and intravenously injected into mice undergoing transient renal artery occlusion followed by reperfusion (*81*). Persistent contrast enhancement of the postischemic kidney was noted on ultrasound imaging,

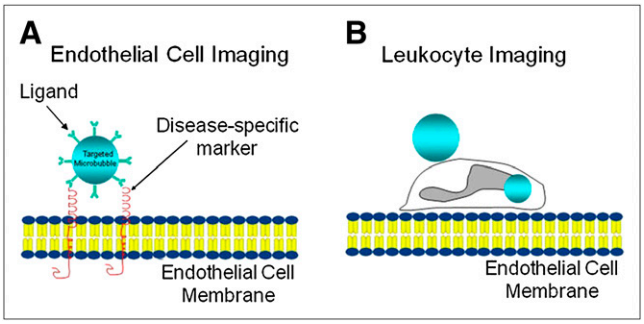

FIGURE 12. Schematic of vascular endothelium and approaches for ultrasound molecular imaging of inflammation during ischemia and reperfusion using microbubble attachment to endothelial cells. (A) Microbubbles bearing targeting ligand on surface can bind to specific endothelial target, such as leukocyte adhesion molecule. (B) Activated leukocytes may bind or phagocytose microbubbles and become acoustically active. Figure not drawn to scale.

which was not seen after the injection of nontargeted bubbles, or after the injection of targeted and nontargeted bubbles into normal control mice. These studies established the concept that P-selectin targeting with an ultrasound contrast agent is a feasible approach for detecting postischemic tissue during ultrasound imaging.

P-selectin targeting for the detection of antecedent myocardial ischemia has been recently described using microbubbles bearing the naturally occurring ligand for selectins. The major ligands for all 3 selectins are cell surface glycans possessing a specific sialyl Lewis^x (sLe^x) epitope, meaning that a single moiety could theoretically be used to target both P- and E-selectin, which are expressed early and late, respectively, after reperfusion (*87*). Sialyl-Lewis^x was conjugated to the surface of lipid microbubbles and initially tested for adhesive properties under direct visualization during intravital microscopy of rat cremaster microcirculation rendered inflammatory by intrascrotal tumor necrosis factor-α administration (*82*). Sialyl-Lewis^x microbubbles adhered to activated endothelium, whereas control Le^x-conjugated microbubbles minimally adhered, with neither bubble species adhering significantly to normal, noninflamed endothelium. A rat model of myocardial ischemia and reperfusion was then used to echocardiographically detect adhesion events (*82*). Both early (30 min) and late (up to 90 min) after reflow, video intensity in the postischemic bed after the intravenous injection of sLe^x microbubbles was significantly higher than that in the nonischemic bed. Furthermore, the region of persistent contrast enhancement colocalized with, and correlated in size to, the risk area (Fig. 13). There was also a trend toward similar findings after milder (10 min) ischemia. These data indicate that the selectin-targeted microbubbles are capable of recapitulating the presence, location, and spatial extent of previously ischemic myocardium.

As mentioned previously, another approach to inflammatory imaging for the detection of prior ischemia is the use of microbubbles that are avid for activated leukocytes. Lipid microbubbles augmented with phosphatidylserine in the shell adhere to activated leukocytes (*41*) and remain acoustically active even after leukocyte phagocytosis (*86*). Phosphatidylserine microbubbles have been intravenously injected into canines with reperfused myocardial infarction, and ultrasound imaging demonstrated persistent contrast enhancement in the region of prior ischemia and infarction (Fig. 14) (*88*). Note that this approach appears feasible in

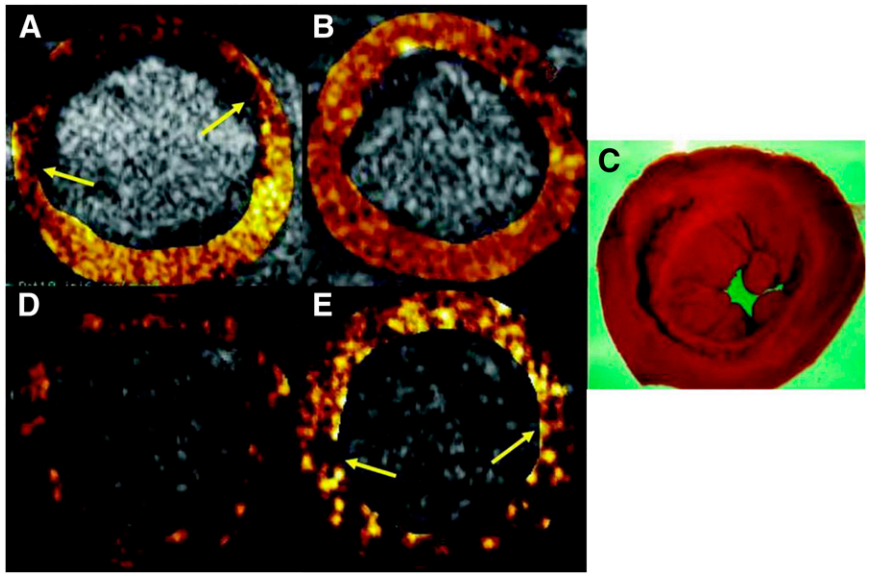

FIGURE 13. Ultrasound ischemic memory imaging of myocardium using microbubbles targeted to bind to P-selectin via tetrasaccharide sialyl Lewis^x in rat model of 15-min coronary occlusion followed by reperfusion. Short-axis nonlinear ultrasound images of heart are background-subtracted, and degree of contrast enhancement is color-coded. (A) Injection of nontargeted microbubbles during coronary occlusion shows risk area (region between arrows). (B) After reperfusion, nontargeted microbubble injection confirms restoration of myocardial perfusion. (C) Postmortem staining with triphenyl tetrazolium chloride (TTC) indicates no infarction. (D) Delayed imaging after injection of control microbubbles during reperfusion demonstrates no persistent contrast enhancement. (E) Delayed imaging after injection of P-selectin–targeted microbubbles during reperfusion shows persistent contrast enhancement in region that was previously ischemic (risk area, A). (Adapted with permission of (*82*).)

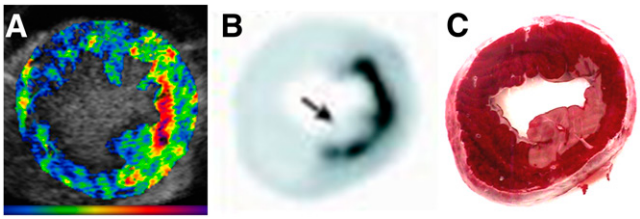

FIGURE 14. Inflammatory imaging of reperfused infarcted canine myocardium using phosphatidylserine-augmented lipid microbubbles that attach to activated leukocytes. Short-axis nonlinear ultrasound images are background-subtracted and color-coded. (A) After injection of leukocyte-avid microbubbles during reperfusion, note persistent contrast enhancement of previously ischemic area. (B) Confirmation of leukocyte accumulation in postischemic zone on autoradiography of isotope-labeled leukocytes. (C) TTC-stained myocardial specimen demonstrates nontransmural infarction (*88*).

a model in which there is sizeable infarction; it is unclear whether a leukocyte-avid microbubble would be effective in delineating antecedent ischemia in which there is minimal or only mild necrosis, the clinical scenarios in which the emergency department evaluation of chest pain is particularly problematic.

Future Directions and Challenges

Ultrasonic identification of acute adhesion molecule expression or leukocyte activation on postischemic endothelium could enable not only the identification of recent myocardial ischemia but also the mapping of its location and spatial extent. The ability to causally link a discrete episode of chest pain to true myocardial ischemia would be a powerful clinical tool for the triage and subsequent testing of patients presenting with symptoms and clinical signs suggestive, but not diagnostic, of coronary ischemia. Further studies will be required to establish whether this approach is incremental to existing diagnostic clinical tools. Furthermore, the time window for useful imaging, and sensitivity to varying degrees and durations of ischemia, need to be defined.

The clinical translation of the concepts described here has challenges that are inherent to ultrasound molecular imaging in general. Targeting ligands need to be nonimmunogenic (e.g., not monoclonal antibodies), with adhesive kinetics that are optimized for attachment and persistence on the endothelium. Maximal sensitivity for detection will require both optimized adhesive dynamics, which may include multitargeting and selection of ligands with better on–off rates to permit maximal microbubble adhesion, and imaging systems that can detect acoustic signals unique to adhered microbubbles, as opposed to those that are freely circulating. Such requirements will demand that multidisciplinary efforts be used to bring these promising developments to clinical fruition.

CHALLENGES AND FUTURE NEEDS FOR IMAGING MYOCARDIAL METABOLIC REMODELING

As seen in the preceding discussion, metabolic imaging using a variety of technologies is playing a key role in delineating the relationship between myocardial metabolic remodeling and cardiovascular disease. However, for metabolic imaging to achieve its full potential, advances in several areas must occur. First, there must be continued improvement in instrumentation design, acquisition schemes, and image analysis methods that permit quantitative measurements of metabolic processes of interest that are accurate, robust, and reproducible, and that are capable of being performed in both rodents and humans. There is a compelling need for the development of new radiopharmaceuticals and contrast agents that permit characterization of key metabolic pathways such as uptake, storage, or oxidation that are linked to disease manifestations. Moreover, new imaging agents are needed to provide insights into the detrimental effects on myocellular health of perturbations in myocardial metabolism, such as activation of inflammatory, oxidative stress, cell growth, and cell survival pathways. Ultimately, appropriately powered clinical trials will need to be performed to determine whether the metabolic signatures identified by imaging in various diseases provide unique information that will alter the care of the cardiac patient.

ACKNOWLEDGMENTS

This work was supported in part by grants P01-HL13851 and HL69100 (RJG), R37HL49244, R01HL62702, R01HL56178 (EDL), and R01HL077434 (FSV) from the National Institutes of Health.

REFERENCES

1. Taegtmeyer H. Tracing cardiac metabolism in vivo: one substrate at a time. *J Nucl Med.* 2010:51:5(suppl):80–87.
2. He ZX, Shi RF, Wu YJ, et al. Direct imaging of exercise-induced myocardial ischemia with fluorine-18-labeled deoxyglucose and Tc-99m-sestamibi in coronary artery disease. *Circulation.* 2003;108:1208–1213.
3. Bergmann SR, Weinheimer CJ, Markham J, Herrero P. Quantitation of myocardial fatty acid metabolism using PET. *J Nucl Med.* 1996;37:1723–1730.
4. Herrero P, Dence CS, Coggan AR, Kisrieva-Ware Z, Eisenbeis P, Gropler RJ. L-3-^{11}C-lactate as a PET tracer of myocardial lactate metabolism: a feasibility study. *J Nucl Med.* 2007;48:2046–2055.
5. Herrero P, Kisrieva-Ware Z, Dence CS, et al. PET measurements of myocardial glucose metabolism with 1-^{11}C-glucose and kinetic modeling. *J Nucl Med.* 2007; 48:955–964.
6. Hudsmith LE, Neubauer S. Magnetic resonance spectroscopy in myocardial disease. *JACC Cardiovasc Imaging.* 2009;2:87–96.
7. Ingwall JS. Energy metabolism in heart failure and remodeling. *Cardiovasc Res.* 2009;81:412–419.
8. Lewandowski ED. Cardiac carbon-13 magnetic resonance spectroscopy: on the horizon or over the rainbow? *J Nucl Cardiol.* 2002;9:419–428.
9. Griffin JL, White LT, Lewandowski ED. Substrate-dependent proton load and recovery of stunned hearts during pyruvate dehydrogenase stimulation. *Am J Physiol Heart Circ Physiol.* 2000;279:H361–H367.
10. Sorokina N, O'Donnell JM, McKinney RD, et al. Recruitment of compensatory pathways to sustain oxidative flux with reduced carnitine palmitoyltransferase I activity characterizes inefficiency in energy metabolism in hypertrophied hearts. *Circulation.* 2007;115:2033–2041.

11. Di Carli MF, Asgarzadie F, Schelbert HR, et al. Quantitative relation between myocardial viability and improvement in heart failure symptoms after revascularization in patients with ischemic cardiomyopathy. *Circulation.* 1995;92: 3436–3444.
12. Di Carli MF, Davidson M, Little R, et al. Value of metabolic imaging with positron emission tomography for evaluating prognosis in patients with coronary artery disease and left ventricular dysfunction. *Am J Cardiol.* 1994;73:527–533.
13. Eitzman D, al-Aouar Z, Kanter HL, et al. Clinical outcome of patients with advanced coronary artery disease after viability studies with positron emission tomography. *J Am Coll Cardiol.* 1992;20:559–565.
14. Tillisch J, Brunken R, Marshall R, et al. Reversibility of cardiac wall-motion abnormalities predicted by positron tomography. *N Engl J Med.* 1986;314:884–888.
15. Allman KC, Shaw LJ, Hachamovitch R, Udelson JE. Myocardial viability testing and impact of revascularization on prognosis in patients with coronary artery disease and left ventricular dysfunction: a meta-analysis. *J Am Coll Cardiol.* 2002;39:1151–1158.
16. Dilsizian V, Rocco TP, Freedman NM, Leon MB, Bonow RO. Enhanced detection of ischemic but viable myocardium by the reinjection of thallium after stress-redistribution imaging. *N Engl J Med.* 1990;323:141–146.
17. Srinivasan G, Kitsiou AN, Bacharach SL, Bartlett ML, Miller-Davis C, Dilsizian V. [^{18}F]fluorodeoxyglucose single photon emission computed tomography: can it replace PET and thallium SPECT for the assessment of myocardial viability? *Circulation.* 1998;97:843–850.
18. Bax JJ, Visser FC, Blanksma PK, et al. Comparison of myocardial uptake of fluorine-18-fluorodeoxyglucose imaged with PET and SPECT in dyssynergic myocardium. *J Nucl Med.* 1996;37:1631–1636.
19. Burt RW, Perkins OW, Oppenheim BE, et al. Direct comparison of fluorine-18-FDG SPECT, fluorine-18-FDG PET and rest thallium-201 SPECT for detection of myocardial viability. *J Nucl Med.* 1995;36:176–179.
20. Sandler MP, Videlefsky S, Delbeke D, et al. Evaluation of myocardial ischemia using a rest metabolism/stress perfusion protocol with fluorine-18 deoxyglucose/ technetium-99m MIBI and dual-isotope simultaneous-acquisition single-photon emission computed tomography. *J Am Coll Cardiol.* 1995;26:870–878.
21. Dilsizian V, Bacharach SL, Khin MM, Smith MF. Fluorine-18-deoxyglucose SPECT and coincidence imaging for myocardial viability: clinical and technologic issues. *J Nucl Cardiol.* 2001;8:75–88.
22. Dilsizian V, Bateman TM, Bergmann SR, et al. Metabolic imaging with beta-methyl-p-[^{123}I]-iodophenyl-pentadecanoic acid identifies ischemic memory after demand ischemia. *Circulation.* 2005;112:2169–2174.
23. Kawai Y, Tsukamoto E, Nozaki Y, Morita K, Sakurai M, Tamaki N. Significance of reduced uptake of iodinated fatty acid analogue for the evaluation of patients with acute chest pain. *J Am Coll Cardiol.* 2001;38:1888–1894.
24. Buxton DB, Mody FV, Krivokapich J, Phelps ME, Schelbert HR. Quantitative assessment of prolonged metabolic abnormalities in reperfused canine myocardium. *Circulation.* 1992;85:1842–1856.
25. Taegtmeyer H, Dilsizian V. Imaging myocardial metabolism and ischemic memory. *Nat Clin Pract Cardiovasc Med.* 2008;5(suppl 2):S42–S48.
26. Dou KF, Yang MF, Yang YJ, Jain D, He ZX. Myocardial ^{18}F-FDG uptake after exercise-induced myocardial ischemia in patients with coronary artery disease. *J Nucl Med.* 2008;49:1986–1991.
27. Gropler RJ, Siegel BA, Lee KJ, et al. Nonuniformity in myocardial accumulation of fluorine-18-fluorodeoxyglucose in normal fasted humans. *J Nucl Med.* 1990; 31:1749–1756.
28. Kontos MC, Dilsizian V, Weiland F, et al. Iodofiltic acid I-123 (BMIPP) fatty acid imaging improves initial diagnosis in emergency department patients with suspected acute coronary syndromes: a multicenter trial. *J Am Coll Cardiol.* 2010. In press.
29. Nishimura M, Hashimoto T, Kobayashi H, et al. Myocardial scintigraphy using a fatty acid analogue detects coronary artery disease in hemodialysis patients. *Kidney Int.* 2004;66:811–819.
30. Nishimura M, Tsukamoto K, Hasebe N, Tamaki N, Kikuchi K, Ono T. Prediction of cardiac death in hemodialysis patients by myocardial fatty acid imaging. *J Am Coll Cardiol.* 2008;51:139–145.
31. Dilsizian V, Fink JC. Deleterious effect of altered myocardial fatty acid metabolism in kidney disease. *J Am Coll Cardiol.* 2008;51:146–148.
32. Phelps ME, Hoffman EJ, Selin C, et al. Investigation of [^{18}F]2-fluoro-2-deoxyglucose for the measure of myocardial glucose metabolism. *J Nucl Med.* 1978;19:1311–1319.
33. Schinkel AF, Bax JJ, Poldermans D, Elhendy A, Ferrari R, Rahimtoola SH. Hibernating myocardium: diagnosis and patient outcomes. *Curr Probl Cardiol.* 2007;32:375–410.
34. Beanlands RS, Nichol G, Huszti E, et al. F-18-fluorodeoxyglucose positron emission tomography imaging-assisted management of patients with severe left ventricular dysfunction and suspected coronary disease: a randomized, controlled trial (PARR-2). *J Am Coll Cardiol.* 2007;50:2002–2012.
35. D'Egidio G, Nichol G, Williams KA, et al. Increasing benefit from revascularization is associated with increasing amounts of myocardial hibernation: a substudy of the PARR-2 trial. *JACC Cardiovasc Imaging.* 2009;2:1060–1068.
36. Abraham A, Nichol G, Williams KA, et al. ^{18}F-FDG PET imaging of myocardial viability in an experienced center with access to ^{18}F-FDG and integration with clinical management teams: the Ottawa-FIVE substudy of the PARR-2 trial. *J Nucl Med.* 2010;51:567–574.
37. deKemp RA, Renaud JM, Farncombe T, et al. PET imaging standards for the Ontario Provincial Registry of Cardiac Viability Imaging with FDG PET (CADRE) [abstract]. *J Nucl Med.* 2009;50(suppl 2):290P.
38. Shoghi KI, Gropler RJ, Sharp T, et al. Time course of alterations in myocardial glucose utilization in the Zucker diabetic fatty rat with correlation to gene expression of glucose transporters: a small-animal PET investigation. *J Nucl Med.* 2008;49:1320–1327.
39. Finck BN, Lehman JJ, Leone TC, et al. The cardiac phenotype induced by PPARalpha overexpression mimics that caused by diabetes mellitus. *J Clin Invest.* 2002;109:121–130.
40. Burkart EM, Sambandam N, Han X, et al. Nuclear receptors PPARbeta/delta and PPARalpha direct distinct metabolic regulatory programs in the mouse heart. *J Clin Invest.* 2007;117:3930–3939.
41. Gollob MH, Green MS, Tang AS, et al. Identification of a gene responsible for familial Wolff-Parkinson-White syndrome. *N Engl J Med.* 2001;344:1823–1831.
42. Gollob MH. Glycogen storage disease as a unifying mechanism of disease in the *PRKAG2* cardiac syndrome. *Biochem Soc Trans.* 2003;31:228–231.
43. Thorn S, Lamoureux M, deKemp R, et al. Reduced myocardial uptake and function in ARG302GLN *PRKAG2* mutant mice as measured by FDG PET and echocardiography [abstract]. *Can J Cardiol.* 2008;24(suppl E):p291E.
44. Ha AC, Renaud JM, Dekemp RA, et al. In vivo assessment of myocardial glucose uptake by positron emission tomography in adults with the PRKAG2 cardiac syndrome. *Circ Cardiovasc Imaging.* 2009;2:485–491.
45. Tuunanen H, Kuusisto J, Toikka J, et al. Myocardial perfusion, oxidative metabolism, and free fatty acid uptake in patients with hypertrophic cardiomyopathy attributable to the Asp175Asn mutation in the alpha-tropomyosin gene: a positron emission tomography study. *J Nucl Cardiol.* 2007;14:354–365.
46. Blackledge MJ, Rajagopalan B, Oberhaensli RD, Bolas NM, Styles P, Radda GK. Quantitative studies of human cardiac metabolism by ^{31}P rotating-frame NMR. *Proc Natl Acad Sci USA.* 1987;84:4283–4287.
47. Bottomley PA, Weiss RG, Hardy CJ, Baumgartner WA. Myocardial high-energy phosphate metabolism and allograft rejection in patients with heart transplants. *Radiology.* 1991;181:67–75.
48. Weiss RG, Bottomley PA, Hardy CJ, Gerstenblith G. Regional myocardial metabolism of high-energy phosphates during isometric exercise in patients with coronary artery disease. *N Engl J Med.* 1990;323:1593–1600.
49. Hardy CJ, Weiss RG, Bottomley PA, Gerstenblith G. Altered myocardial high-energy phosphate metabolites in patients with dilated cardiomyopathy. *Am Heart J.* 1991;122:795–801.
50. Jung WI, Sieverding L, Breuer J, et al. ^{31}P NMR spectroscopy detects metabolic abnormalities in asymptomatic patients with hypertrophic cardiomyopathy. *Circulation.* 1998;97:2536–2542.
51. de Roos A, Doornbos J, Luyten PR, Oosterwaal LJ, van der Wall EE, den Hollander JA. Cardiac metabolism in patients with dilated and hypertrophic cardiomyopathy: assessment with proton-decoupled P-31 MR spectroscopy. *J Magn Reson Imaging.* 1992;2:711–719.
52. Smith CS, Bottomley PA, Schulman SP, Gerstenblith G, Weiss RG. Altered creatine kinase adenosine triphosphate kinetics in failing hypertrophied human myocardium. *Circulation.* 2006;114:1151–1158.
53. Lewandowski ED, Kudej RK, White LT, O'Donnell JM, Vatner SF. Mitochondrial preference for short chain fatty acid oxidation during coronary artery constriction. *Circulation.* 2002;105:367–372.
54. Malloy CR, Sherry AD, Jeffrey FM. Analysis of tricarboxylic acid cycle of the heart using ^{13}C isotope isomers. *Am J Physiol.* 1990;259:H987–H995.
55. Griffin JL, O'Donnell JM, White LT, Hajjar RJ, Lewandowski ED. Postnatal expression and activity of the mitochondrial 2-oxoglutarate-malate carrier in intact hearts. *Am J Physiol Cell Physiol.* 2000;279:C1704–C1709.
56. Lewandowski ED, O'Donnell JM, Scholz TD, Sorokina N, Buttrick PM. Recruitment of NADH shuttling in pressure-overloaded and hypertrophic rat hearts. *Am J Physiol Cell Physiol.* 2007;292:C1880–C1886.
57. Banke NH, Leone TC, Kelly DP, Lewandowski ED. Accelerated triacylglyceride dynamics induced by cardiac PPARα overexpression are potentiated by

adrenergic stress to reveal increased reliance on endogenous lipid stores [abstract]. *Circulation.* 2008;118(suppl):S539.
58. Lehman JJ, Boudina S, Banke NH, et al. The transcriptional coactivator PGC-1alpha is essential for maximal and efficient cardiac mitochondrial fatty acid oxidation and lipid homeostasis. *Am J Physiol Heart Circ Physiol.* 2008;295: H185–H196.
59. O'Donnell JM, Fields AD, Sorokina N, Lewandowski ED. The absence of endogenous lipid oxidation in early stage heart failure exposes limits in lipid storage and turnover. *J Mol Cell Cardiol.* 2008;44:315–322.
60. Pound KM, Sorokina N, Ballal K, et al. Substrate-enzyme competition attenuates upregulated anaplerotic flux through malic enzyme in hypertrophied rat heart and restores triacylglyceride content: attenuating upregulated anaplerosis in hypertrophy. *Circ Res.* 2009;104:805–812.
61. Merritt ME, Harrison C, Storey C, Jeffrey FM, Sherry AD, Malloy CR. Hyperpolarized ^{13}C allows a direct measure of flux through a single enzyme-catalyzed step by NMR. *Proc Natl Acad Sci USA.* 2007;104:19773–19777.
62. Schroeder MA, Atherton HJ, Cochlin LE, Clarke K, Radda GK, Tyler DJ. The effect of hyperpolarized tracer concentration on myocardial uptake and metabolism. *Magn Reson Med.* 2009;61:1007–1014.
63. Schroeder MA, Cochlin LE, Heather LC, Clarke K, Radda GK, Tyler DJ. In vivo assessment of pyruvate dehydrogenase flux in the heart using hyperpolarized carbon-13 magnetic resonance. *Proc Natl Acad Sci USA.* 2008;105:12051–12056.
64. McGavock JM, Lingvay I, Zib I, et al. Cardiac steatosis in diabetes mellitus: a ^{1}H-magnetic resonance spectroscopy study. *Circulation.* 2007;116:1170–1175.
65. van der Meer RW, Rijzewijk LJ, de Jong HW, et al. Pioglitazone improves cardiac function and alters myocardial substrate metabolism without affecting cardiac triglyceride accumulation and high-energy phosphate metabolism in patients with well-controlled type 2 diabetes mellitus. *Circulation.* 2009;119: 2069–2077.
66. Rijzewijk LJ, van der Meer RW, Smit JW, et al. Myocardial steatosis is an independent predictor of diastolic dysfunction in type 2 diabetes mellitus. *J Am Coll Cardiol.* 2008;52:1793–1799.
67. Hammer S, van der Meer RW, Lamb HJ, et al. Short-term flexibility of myocardial triglycerides and diastolic function in patients with type 2 diabetes mellitus. *Am J Physiol Endocrinol Metab.* 2008;295:E714–E718.
68. Hankiewicz JH, Banke NH, Lewandowski ED. Myocardial lipid accumulation due to high fat diet in PPAR-alpha overexpressing mouse hearts reduces endocardial 2-D principal strains. Paper presented at: 17th Annual Scientific Meeting of the International Societies for Magnetic Resonance in Medicine; April 2009; Honolulu, HI.
69. Krieglstein CF, Granger DN. Adhesion molecules and their role in vascular disease. *Am J Hypertens.* 2001;14(suppl):44S−54S.
70. Kurose I, Anderson DC, Miyasaka M, et al. Molecular determinants of reperfusion-induced leukocyte adhesion and vascular protein leakage. *Circ Res.* 1994;74:336–343.
71. Ley K, Bullard DC, Arbones ML, et al. Sequential contribution of L- and P-selectin to leukocyte rolling in vivo. *J Exp Med.* 1995;181:669–675.
72. Kaul S. Myocardial contrast echocardiography: a 25-year retrospective. *Circulation.* 2008;118:291–308.
73. Jayaweera AR, Edwards N, Glasheen WP, Villanueva FS, Abbott RD, Kaul S. In vivo myocardial kinetics of air-filled albumin microbubbles during myocardial contrast echocardiography: comparison with radiolabeled red blood cells. *Circ Res.* 1994;74:1157–1165.
74. de Jong N, Bouakaz A, Frinking P. Basic acoustic properties of microbubbles. *Echocardiography.* 2002;19:229–240.
75. Hundley WG, Kizilbash AM, Afridi I, Franco F, Peshock RM, Grayburn PA. Administration of an intravenous perfluorocarbon contrast agent improves echocardiographic determination of left ventricular volumes and ejection fraction: comparison with cine magnetic resonance imaging. *J Am Coll Cardiol.* 1998;32: 1426–1432.
76. Villanueva FS, Abraham JA, Schreiner GF, et al. Myocardial contrast echocardiography can be used to assess the microvascular response to vascular endothelial growth factor-121. *Circulation.* 2002;105:759–765.
77. Villanueva FS, Gertz EW, Csikari M, Pulido G, Fisher D, Sklenar J. Detection of coronary artery stenosis with power Doppler imaging. *Circulation.* 2001;103: 2624–2630.
78. Wei K, Jayaweera AR, Firoozan S, Linka A, Skyba DM, Kaul S. Quantification of myocardial blood flow with ultrasound-induced destruction of microbubbles administered as a constant venous infusion. *Circulation.* 1998;97:473–483.
79. Villanueva FS, Wagner WR. Ultrasound molecular imaging of cardiovascular disease. *Nat Clin Pract Cardiovasc Med.* 2008;5(suppl 2):S26–S32.
80. Leong-Poi H, Christiansen J, Heppner P, et al. Assessment of endogenous and therapeutic arteriogenesis by contrast ultrasound molecular imaging of integrin expression. *Circulation.* 2005;111:3248–3254.
81. Lindner JR, Song J, Christiansen J, Klibanov AL, Xu F, Ley K. Ultrasound assessment of inflammation and renal tissue injury with microbubbles targeted to P-selectin. *Circulation.* 2001;104:2107–2112.
82. Villanueva FS, Lu E, Bowry S, et al. Myocardial ischemic memory imaging with molecular echocardiography. *Circulation.* 2007;115:345–352.
83. Weller GE, Villanueva FS, Tom EM, Wagner WR. Targeted ultrasound contrast agents: in vitro assessment of endothelial dysfunction and multi-targeting to ICAM-1 and sialyl Lewis^{x}. *Biotechnol Bioeng.* 2005;92:780–788.
84. Dayton PA, Chomas JE, Lum AF, et al. Optical and acoustical dynamics of microbubble contrast agents inside neutrophils. *Biophys J.* 2001;80:1547–1556.
85. Lindner JR, Dayton PA, Coggins MP, et al. Noninvasive imaging of inflammation by ultrasound detection of phagocytosed microbubbles. *Circulation.* 2000;102: 531–538.
86. Lindner JR, Song J, Xu F, et al. Noninvasive ultrasound imaging of inflammation using microbubbles targeted to activated leukocytes. *Circulation.* 2000;102:2745–2750.
87. Foxall C, Watson SR, Dowbenko D, et al. The three members of the selectin receptor family recognize a common carbohydrate epitope, the sialyl Lewis(x) oligosaccharide. *J Cell Biol.* 1992;117:895–902.
88. Christiansen JP, Leong-Poi H, Klibanov AL, Kaul S, Lindner JR. Noninvasive imaging of myocardial reperfusion injury using leukocyte-targeted contrast echocardiography. *Circulation.* 2002;105:1764–1767.